Stanford Exploration Project, Report 75, November 17, 1997, pages 167–181

Phase shift datuming and migration from an irregular surface

Jun Ji and Jon Claerbout[1]

keywords: *modeling, algorithm, phase, least squares*

ABSTRACT

We present a phase shift datuming and migration algorithm for the data acquired on a nonflat surface. First of all, we formulate the exploding reflector modeling scheme for a nonflat recording surface. Then, the migration scheme is found as the conjugate operator of the modeling operator. In order to get the correct migration and datuming operators, the forward modeling must be physically reasonable because the conjugate operators are strongly dependent on the forward modeling operator. The artifacts caused by the non-unitary property of the operators can be reduced by a least-squares optimization technique.

INTRODUCTION

Seismic data acquired in areas with irregular topography introduce a numerical problem for migration algorithms that are based on depth extrapolation. Since numerically efficient migration schemes start on a flat interface, wave equation datuming is required prior to the migration. An accurate solution to the problem of varying elevation is to propagate the wavefield from the recording surface to a specified flat datum using wave equation datuming (Berryhill, 1979). Wave-equation datuming (Berryhill, 1979, 1984) has several applications in seismic data processing –horizon flattening, layer replacement, and forward modeling– which can be performed on either unstacked or stacked data. The computationally expensive datuming procedure is often replaced by a simple time shift for the elevation to datum correction. This simple time shift, or elevation static correction, cannot properly reposition wide angle or steeply dipping reflections.

A simple technique to correct for the error caused by the static time shift was introduced by the "zero velocity layer" concept (Beasley and Lynn, 1989). This technique, however, cannot even be applied to the computationally attractive phase-shift algorithms, because it includes the nonphysical characteristic of zero velocity.

[1]**email:** not available

This paper presents phase-shift datuming and migration techniques for data acquired on any irregular surface.

DATUMING AND DEPTH MIGRATION

Datuming is a method of processing to extrapolate a known wavefield at a specified datum of arbitrary shape to another specified datum, also of arbitrary shape. Often, people think of datuming as a different process than migration. Since most migration schemes are performed by wavefield extrapolation followed by imaging, the datuming is done implicitly during the migration process. The migration process usually does not save any wavefield during the extrapolation because its intended output is the subsurface image.

Examining the relations between the inputs and outputs of datuming and migration operators (Figure 1) helps to understand their similarities. The input to the datuming operator is a wavefield on a specified datum and the output is a wavefield on another datum. The datuming operator is an extrapolation operator in either the depth or the time direction. The migration operator has more components: the imaging and the transformation operators, because it requires the output to be the subsurface image and the image space differs from the data space.

The direction of wavefield extrapolation can be either time or depth. We confine our discussion to depth extrapolation methods using phase shift in this paper.

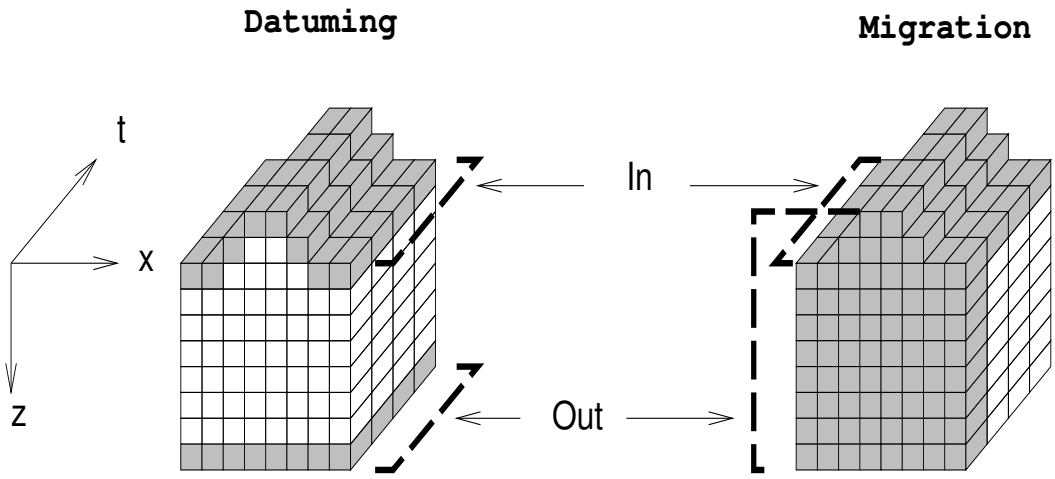

Figure 1: Schematic comparison between the datuming and the depth migration in the input and the output relations. jun1-dtimg [NR]

THE FORWARD OPERATOR AND ITS CONJUGATE

A migration operator is conjugate to the corresponding forward modeling operator (Claerbout, 1992). In order to find the conjugate operator, the linear forward modeling operator must be found first. For the sake of simplicity, we formulate the modeling algorithm from the datuming viewpoint, which requires only an extrapolation operator. The migration operator can be obtained by changing the input from the wavefield to the subsurface image and adding the imaging and transformation operator into the extrapolation operator.

To start, we formulate a simple modeling algorithm using phase-shift extrapolation when the recording surface is not flat. For simplicity, the number of geophone groups on an irregular surface is eight as illustrated in Figure 2.

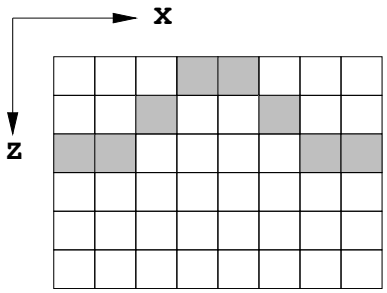

Figure 2: Synthetic surface recording geometry. Solid squares represent geophone location on an undulating surface. jun1-syngeometry [NR]

The wavefield recorded at each geophone is the wavefield propagated up to the depth level where the geophones are located. Therefore, the modeling can be formulated by propagating the wavefield upward without regard for the irregular surface boundary. Then at each altitude, various portions (shaded in Figure 2) are extracted from the wavefield. The sum of these extracted portions makes up the wavefield along the irregular surface. Figure 3 explains this modeling algorithm in the datuming sense.

In order to find the conjugate operator of the algorithm shown in Figure 3, the algorithm must be written down in algebraic form. The algebraic representation for the forward modeling scheme in Figure 3 is given by

$$\begin{bmatrix} A & B & C \end{bmatrix} \begin{bmatrix} FT^* & & \\ & FT^* & \\ & & FT^* \end{bmatrix} \begin{bmatrix} U_1 \\ U_2 \\ U_3 \end{bmatrix} \begin{bmatrix} D_{\text{datum}} \end{bmatrix} = \begin{bmatrix} d_{\text{surface}} \end{bmatrix} \tag{1}$$

$$\begin{aligned} U_1 &= W_3 \\ U_2 &= W_2 W_3 \\ U_3 &= W_1 W_2 W_3, \end{aligned}$$

where D_{datum} and d_{surface} represent the wavefield in the frequency-wavenumber domain at the datum just below the deepest geophone location and the wavefield in the frequency-space domain at the nonflat surface, respectively, and where A,B, and C

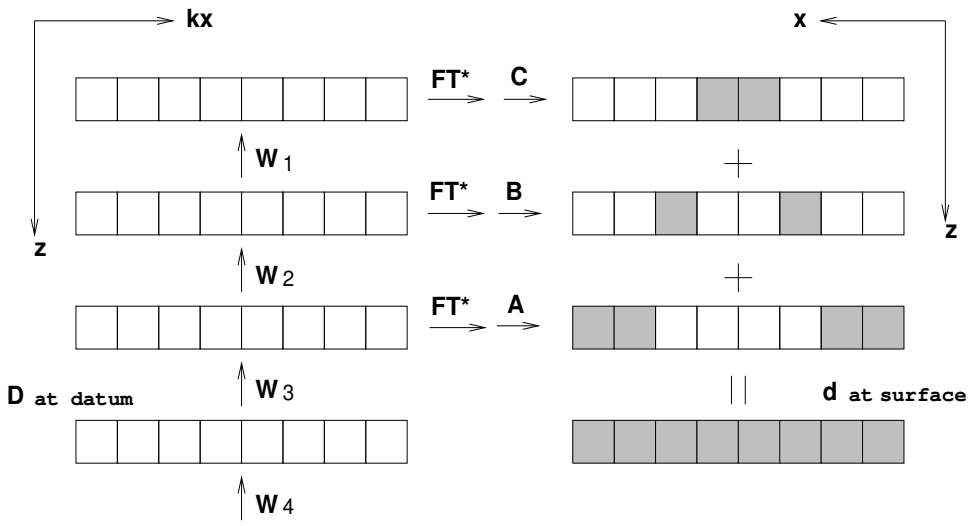

Figure 3: Modeling scheme 1: The schematic diagram for exploding reflector modeling when the surface is not flat. W_j represents the upward propagating operator at the j-th depth level shown in equation (2), FT^* represents the inverse Fourier transform. A, B and C are spatial filter shown in equation (3). jun1-tpmdlschm1 [NR]

are masking operators defined in Figure 3 (and later in equation (2)). Equation (1) shows that the modeling can be decomposed into three steps. The first step is the extrapolation step. The first matrix multiplied to the input has three diagonal matrices, U_1, U_2 and U_3, along its column for the given model and the number of matrices will change as the topography changes. The matrix U_j consists of j operators, from W_j to W_1, which do extrapolation by phase shift from j-th depth level to the surface. The extrapolation operator at each depth level W_j is a diagonal matrix such as:

$$\begin{bmatrix} \exp^{ik_{z_j}\Delta z} & . & . & . & . & . & . & . \\ . & \exp^{ik_{z_j}\Delta z} & . & . & . & . & . & . \\ . & . & \exp^{ik_{z_j}\Delta z} & . & . & . & . & . \\ . & . & . & \exp^{ik_{z_j}\Delta z} & . & . & . & . \\ . & . & . & . & \exp^{ik_{z_j}\Delta z} & . & . & . \\ . & . & . & . & . & \exp^{ik_{z_j}\Delta z} & . & . \\ . & . & . & . & . & . & \exp^{ik_{z_j}\Delta z} & . \\ . & . & . & . & . & . & . & \exp^{ik_{z_j}\Delta z} \end{bmatrix}$$

where k_z is a function of frequency(ω) and horizontal wavenumber(k_x), defined by the dispersion relation of the acoustic wave equation. Some of these elements will be set to zero instead of $\exp^{ik_z\Delta z}$ if k_z falls into an evanescent branch of the dispersion relation. The second step is to inverse Fourier transform along the horizontal axis x in preparation for the third step in which the wavefield is picked where a geophone is located at each depth level. The operator applied in the third step in equation (1) consists of three diagonal matrices on each of which is designed to pick out the

wavefield at the geophone location on each depth level. For the synthetic model given in Figure 2, A, B and C have the following form:

$$A = \begin{bmatrix} 1 & & & & & & \\ & 1 & & & & & \\ & & . & & & & \\ & & & . & & & \\ & & & & . & & \\ & & & & & 1 & \\ & & & & & & 1 \end{bmatrix}, \quad B = \begin{bmatrix} . & & & & & & \\ & . & & & & & \\ & & 1 & & & & \\ & & & . & & & \\ & & & & . & & \\ & & & & & 1 & \\ & & & & & & . \end{bmatrix}$$

$$\text{and} \quad \mathrm{C} = \begin{bmatrix} . & & & & & & \\ & . & & & & & \\ & & . & & & & \\ & & & 1 & & & \\ & & & & 1 & & \\ & & & & & . & \\ & & & & & & . \end{bmatrix} \tag{2}$$

where dots represent zeros.

Now, the datuming operator can be easily found by transposing and taking the complex conjugate of the forward operator shown in equation (1). Therefore, we get the datuming operator for the data gathered on an irregular surface as

$$\begin{bmatrix} U_1^T & U_2^T & U_3^T \end{bmatrix} \begin{bmatrix} FT & & \\ & FT & \\ & & FT \end{bmatrix} \begin{bmatrix} A \\ B \\ C \end{bmatrix} \begin{bmatrix} d_{surface} \end{bmatrix} = \begin{bmatrix} D_{datum} \end{bmatrix} \tag{3}$$

$$\begin{aligned} U_1^T &= W_3^T \\ U_2^T &= W_3^T W_2^T \\ U_3^T &= W_3^T W_2^T W_1^T. \end{aligned}$$

where FT is the Fourier transform along the horizontal axis and W_j^T represents downward phase-shift operator at each depth level. Equation (3) says that the conjugate operator of wavefield picking at several depth levels is the summation of the wavefields which are separately extrapolated from those depth levels at the point where the wavefields were picked. Figure 4 shows a schematic of this datuming operator.

Examples

Figure 5 contains a simple model consisting of a syncline reflector under an undulating surface. The modeling experiment was done using the algorithm explained in Figure 3

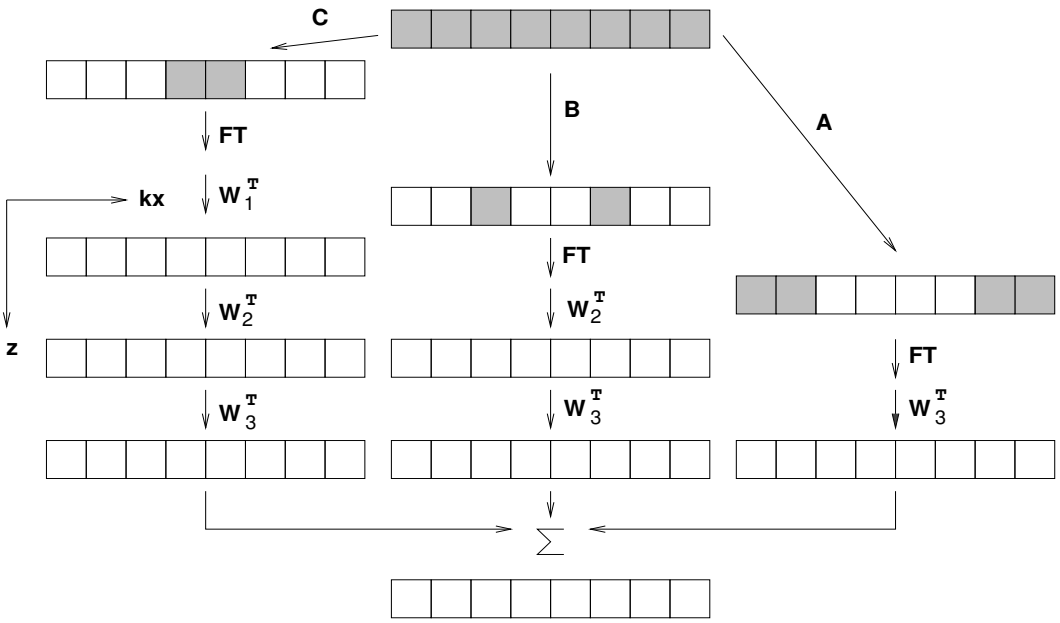

Figure 4: Datuming scheme 1 : Schematic diagram for datuming when the surfaces are irregular as the conjugate operator to modeling scheme 1. W_1^T represents the downward propagation operator at each depth level. jun1-tpmigschm1 [NR]

for a constant velocity and the result is shown in Figure 6(b). During the modeling, we save a wavefield at the bottom of the topography (Figure 6(a)). Comparing these two wavefields, we can see the effect of the irregular topography, the wavefield has a big discontinuity at the center and fluctuates on the right half because of the surface topography. Migration was performed using the algorithm shown in Figure 4 and the results are shown in Figure 6(d). We can see that the syncline reflector is correctly imaged, but there is background noise. During the migration, we saved a wavefield at the bottom of the topography and it is shown in the Figure 6(c). This Figure shows artifacts due to inaccuracies in the extrapolation algorithm. The noise comes mainly from the inaccuracies of the modeling and the next section presents an improved scheme which simulates nature more closely.

IMPROVING THE OPERATOR BY USE OF A FILTER

In the first method, discussed in the previous section, the wavefield is continuously propagated to the top of the surface after it is recorded at the lower altitude. This is not physically possible because after recording at the surface the wavefield goes through air and the air velocity is negligible compared to the earth velocity. In order to make the modeling realistic, we introduce a filter after each extrapolation to stop the propagation of the wavefield after recording. If the wavefield only has only vertical component, the filter introduced has no special effect. However, there is a

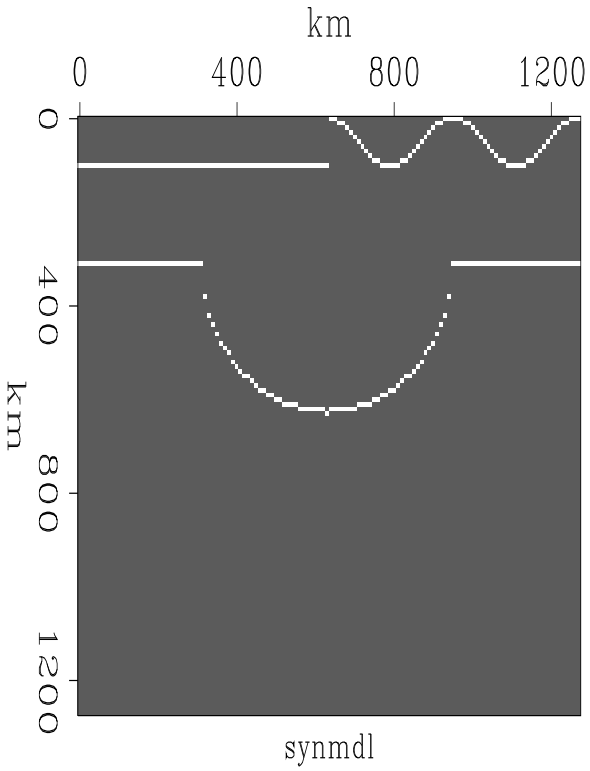

Figure 5: Synthetic model with a syncline reflector image (lower) under an undulating surface (upper). jun1-synmdl [NR]

significant difference between examples with and without the filter when the wavefield has large stepout. The improved scheme by use of the filter is explained schematically in Figure 7.

The scheme shown in Figure 7 can be algebraically formulated as

$$\begin{bmatrix} A & B & C \end{bmatrix} \begin{bmatrix} FT^* & & \\ & FT^* & \\ & & FT^* \end{bmatrix} \begin{bmatrix} U_1 \\ U_2 \\ U_3 \end{bmatrix} \begin{bmatrix} D_{datum} \end{bmatrix} = \begin{bmatrix} d_{surface} \end{bmatrix} \tag{4}$$

$$\begin{aligned} U_1 &= W_3 \\ U_2 &= W_2 FT(I-A)FT^* W_2 \\ U_3 &= W_1 FT(I-A-B)FT^* W_2 FT(I-A)FT^* W_3. \end{aligned}$$

Now, the datuming operator can be found by taking the conjugate transpose operator of the modeling operator in equation (4). Therefore, the improved datuming of the data gathered on an irregular surface is done by

$$\begin{bmatrix} U_1^T & U_2^T & U_3^T \end{bmatrix} \begin{bmatrix} FT & & \\ & FT & \\ & & FT \end{bmatrix} \begin{bmatrix} A \\ B \\ C \end{bmatrix} \begin{bmatrix} d_{surface} \end{bmatrix} = \begin{bmatrix} D_{datum} \end{bmatrix} \tag{5}$$

$$U_1^T = W_3^T$$

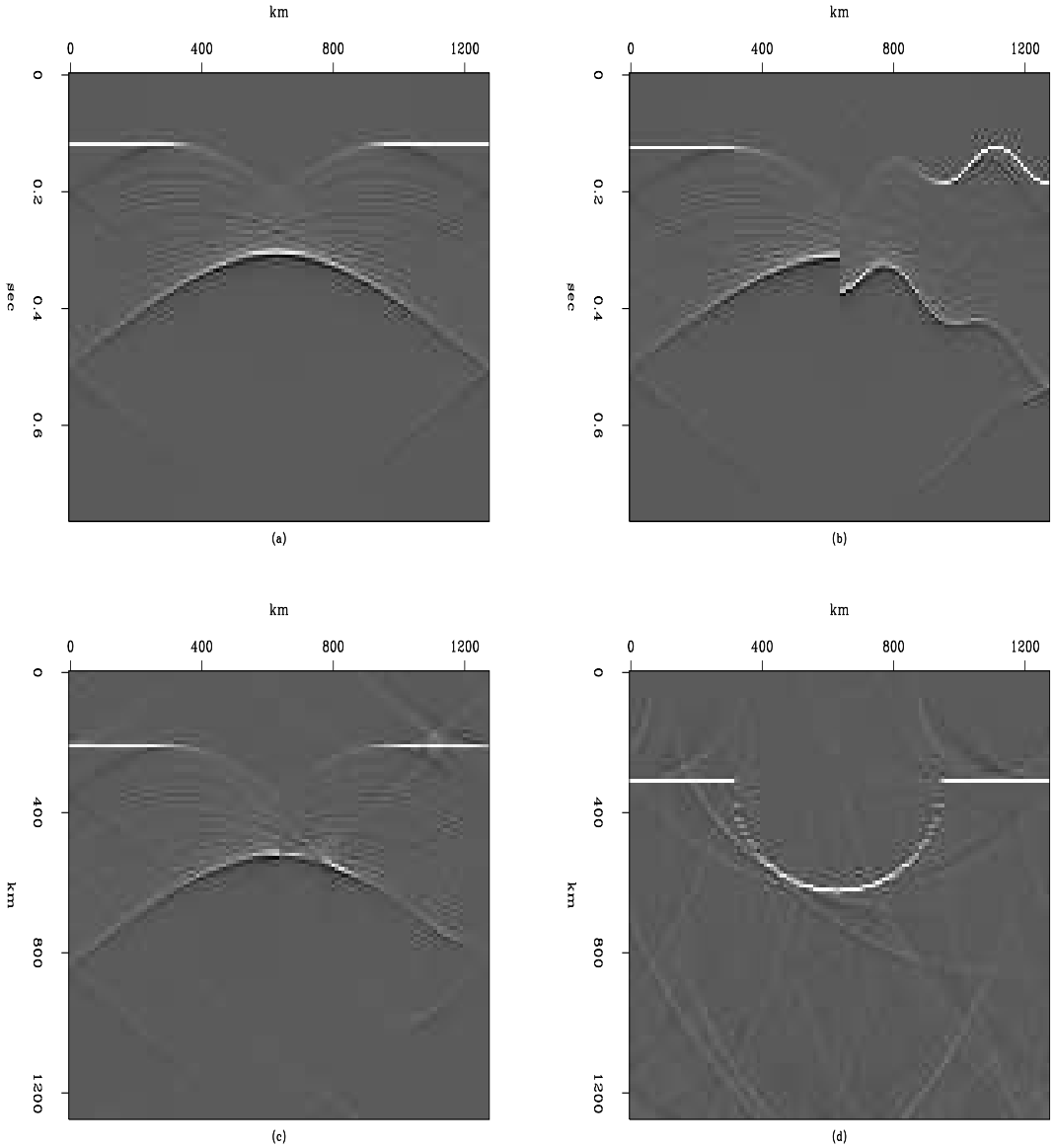

Figure 6: Synthetic examples using the first scheme. **(a)** : Wave field recorded on the depth level at the bottom of the irregular topography. **(b)** : Wave field recorded on the irregular surface. **(c)** : Wave field extrapolated back to the bottom of the topography during the migration. **(d)** : The subsurface image obtained by the migration from the data in Figure 6(b). jun1-dataimgtp1 [NR]

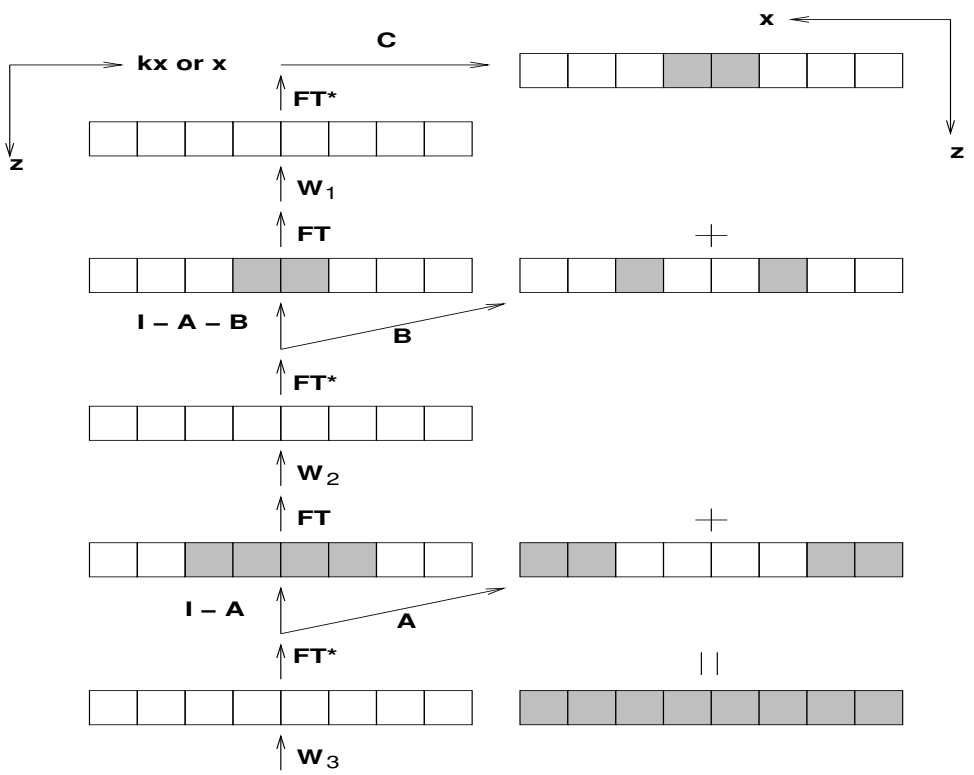

Figure 7:]
Modeling scheme 2 : The schematic diagram for the wavefield extrapolation when the surfaces are irregular with spatial filters that stop the wavefield after recording. W_j represents the upward propagating operator, I is the identity matrix, and A,B and C are matrices in equation (2). [Compare to Figure 3.] jun1-tpmdlschm2 [NR]

$$
\begin{aligned}
U_2^T &= W_3^T FT(I-A)FT^* W_2^T \\
U_3^T &= W_3^T FT(I-A)FT^* W_2^T FT(I-A-B)FT^* W_1^T .
\end{aligned}
$$

The schematic diagram of this datuming operator is given in Figure 8.

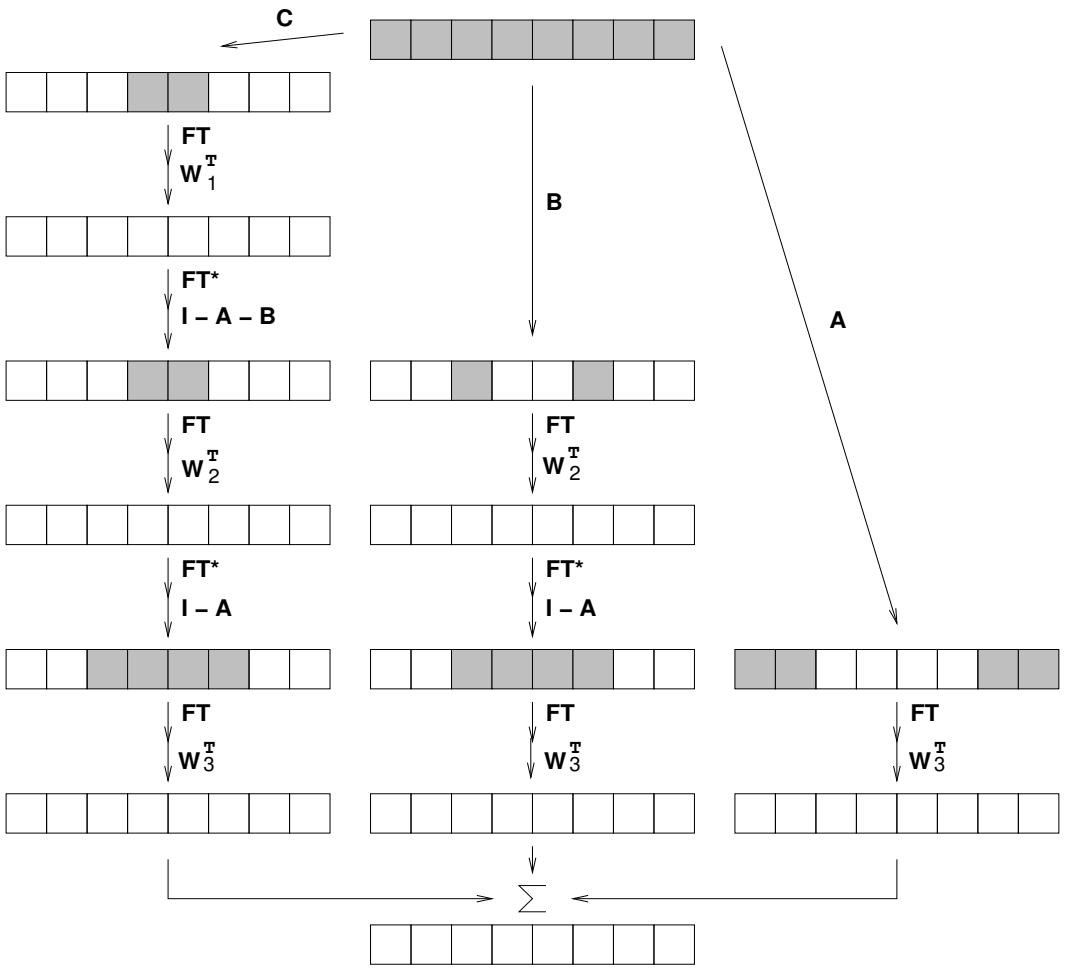

Figure 8:]
Datuming scheme 2 : Schematic diagram for datuming when the surfaces are irregular as the conjugate operator to the modeling scheme 2. W_j^T represents the downward propagating operator. [Compare to Figure 4.] jun1-tpmigschm2 [NR]

Examples

The same synthetic model (Figure 5) that we used in the previous section is used here. The wavefield recorded on the irregular topography in Figure 9(b) clearly demonstrates the effect of the filter. The wavefield traveling vertically does not differ from the result of the first scheme, but the wavefield traveling with some stepout shows differences. In Figure 9(b), the right limb of the bow-tie shows more pronounced

amplitude change which depends on the slope of the surface topography. Locations with the same slope as the stepout of the wavefield does not differ from the result of the first scheme (Figure 6(b)) but the amplitude has been significantly reduced at the locations with the opposite slope of the stepout of the wavefield.

From the result of the migration in Figure 9(d), we can see the noise is suppressed significantly. Comparing to Figure 6(d), the datumed result in the Figure 9(c) has also improved. The datumed wavefield in Figure 9(c) still displays the effect of the irregular topography. There is a big amplitude change at the center and there is a fluctuation of the amplitude along the surface on the right half of the wavefield. This amplitude change along the surface can be explained by the aperture change along the surface caused by the irregular topography. The valley shape topography on the surface will have more aperture compared to the peak shape topography.

LEAST-SQUARES INVERSION

In order to recover the correct amplitude after datuming or migration, we can use the least-squares imaging method introduced by Ji(1992) elsewhere in this report. We use conjugate gradient algorithm. Convergence was obtained in less than five iterations. The right side of Figure 10 shows the datuming inversion result after five iterations. Comparing with the datuming result on the left side in Figure 10, we can see the wavefield is almost the same as the modeled wavefield on the upper left side in Figure 9. The right side of Figure 11 shows the migration inversion result after five iterations of the conjugate gradient algorithm. Comparing with the migration result on the left side in Figure 11, we can see the noise has been reduced and the reflectors are more clearly imaged.

CONCLUSIONS

We present a phase shift datuming and migration algorithm for the data acquired on a nonflat surface. First of all, we formulate the exploding reflector modeling scheme for a nonflat recording surface. Then, the migration scheme is found as the operator conjugate to the modeling operator. In order to get the correct migration and datuming operators, the forward modeling must be physically reasonable because the conjugate operators are strongly dependent on the forward modeling operator. The artifacts caused by the non-unitary property of the operators can be reduced by least-squares optimization technique.

REFERENCES

Beasley, C. J., and Lynn, W., 1989, The zero-velocity layer: Migration from irregular surfaces: Presented at the 59th Ann. Internat. Mtg., Soc. Expl. Geophys.,

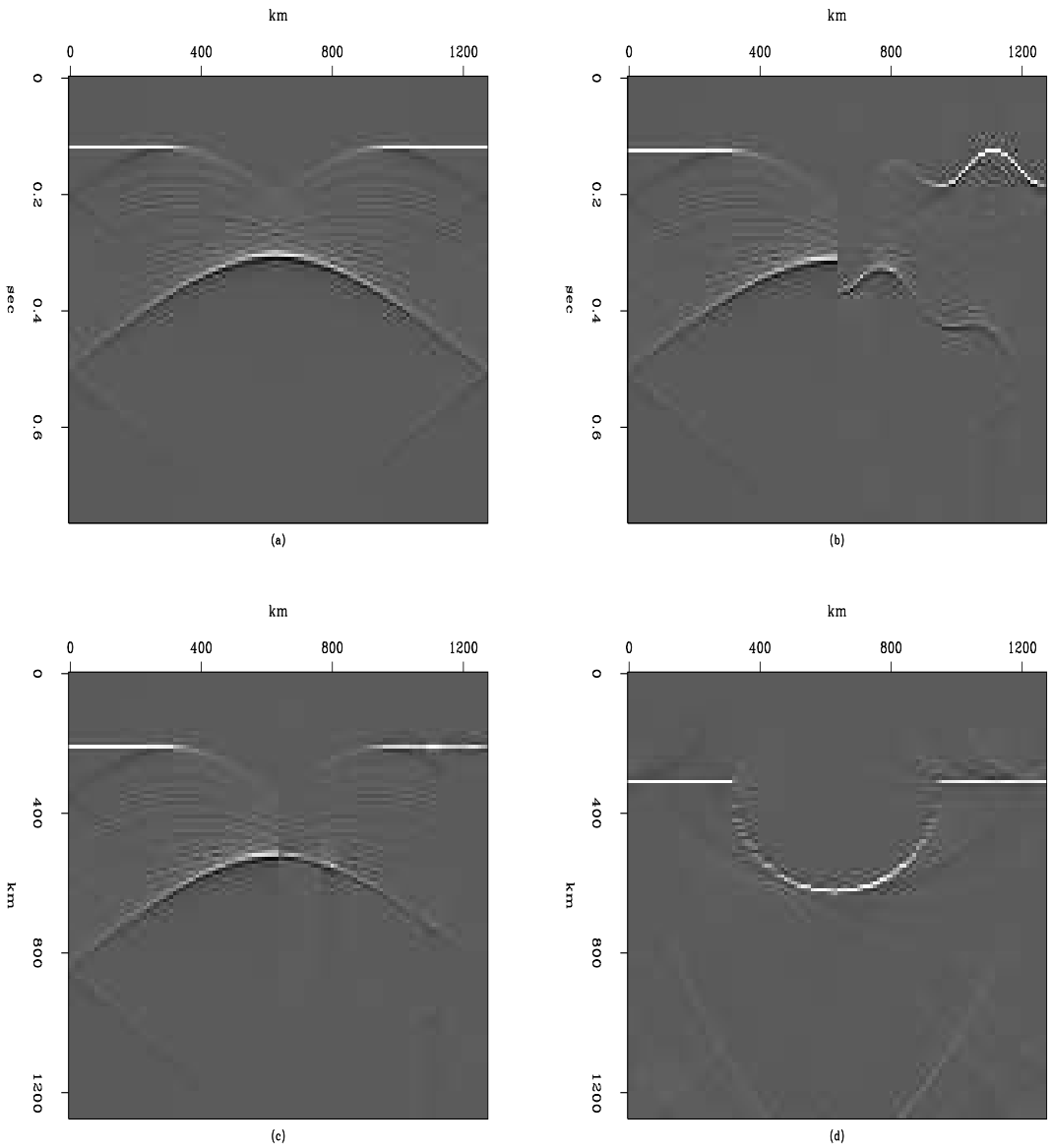

Figure 9:]
Synthetic examples using the second scheme. **(a)** : Wave field recorded at the depth level at the bottom of the irregular topography. **(b)** : Wave field recorded at the irregular surface. **(c)** : Wave field extrapolated back to the bottom of the topography during the migration. **(d)** : The subsurface image obtained by the migration of the data in Figure 9(b). [Compare to Figure 6.] jun1-dataimgtp2 [NR]

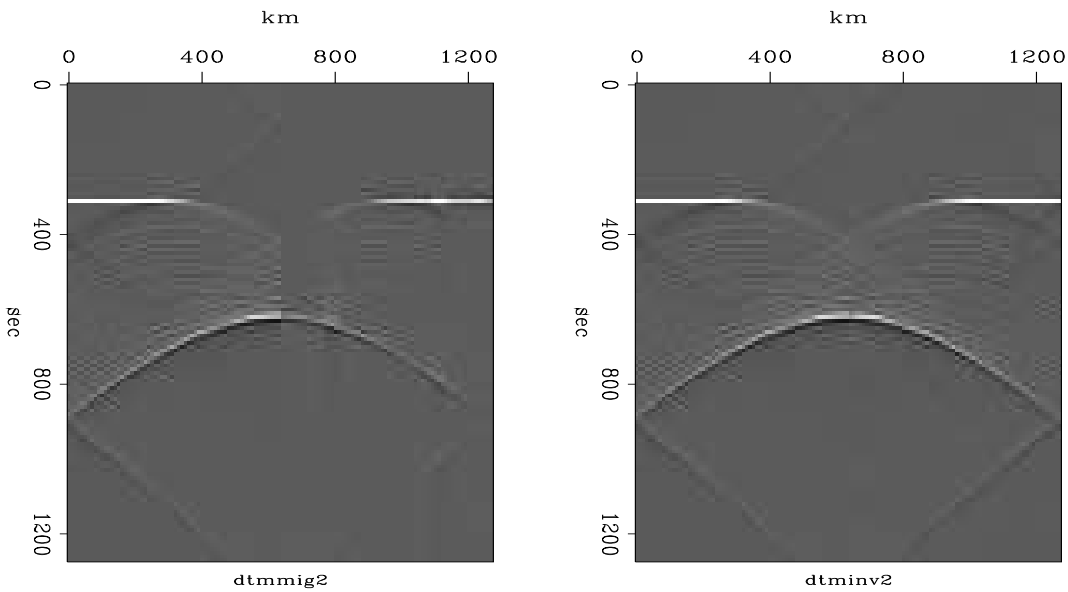

Figure 10: Least squares datuming result for scheme 2. Left : Datuming result by applying the conjugate operator of the modeling (the same as Figure 9(c)). Right : Optimized datuming result by conjugate gradient datuming (after 10 iteration). jun1-datuminv2 [NR]

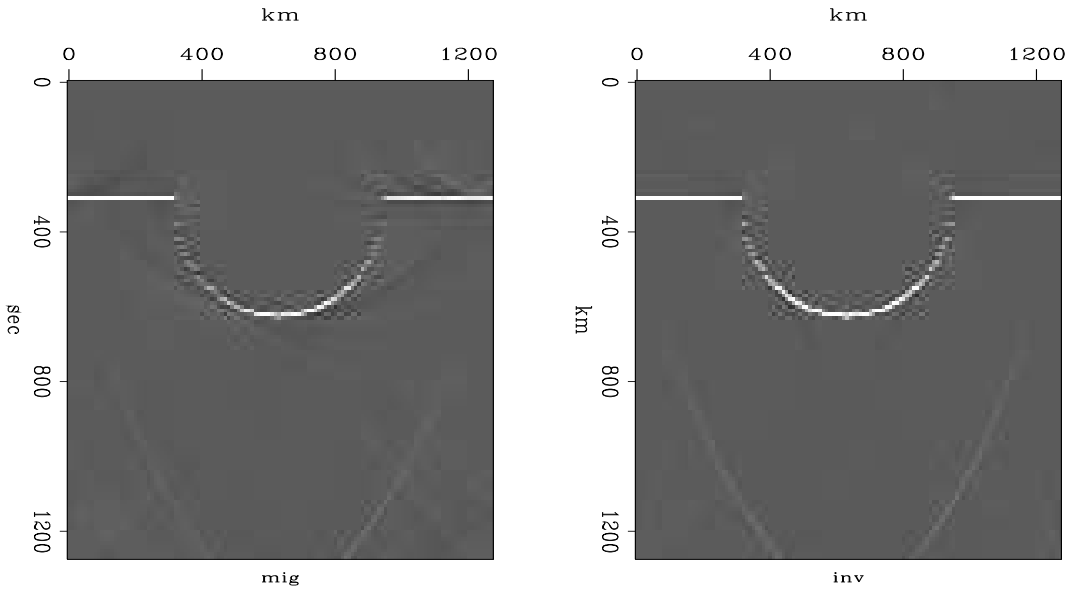

Figure 11: Least squares migration result for scheme 2. Left : Migration result by applying the conjugate operator for the modeling (the same as Figure 9(d)). Right : Optimized migration result by conjugate gradient migration (after 10 iteration). jun1-topomiginv [NR]

Expanded Abstracts, 1179–1183.

Berryhill, R. T., 1979, Wave-equation datuming: Geophysics, **44**, 1329–1344.

Berryhill, R. T., 1984, Wave-equation datuming before stack: Geophysics, **49**, 2064–2066.

Claerbout, J. F., 1992, Earth Soundings Analysis: Processing versus Inversion: Blackwell Scientific.

Ji, J., 1992, Least squares imaging, datuming, and interpolation using the wave equation: SEP **75**, 121–134.